Crystal Structures of Aconitase with Isocitrate and Nitroisocitrate Bound[†,‡]

H. Lauble,[§] M. C. Kennedy,[∥] H. Beinert,[∥] and C. D. Stout*[,§]

Department of Molecular Biology, The Scripps Research Institute, La Jolla, California 92037, and Department of Biochemistry and National Biomedical ESR Center, Medical College of Wisconsin, Milwaukee, Wisconsin 53226

Received September 19, 1991; Revised Manuscript Received December 5, 1991

ABSTRACT: The crystal structures of mitochondrial aconitase with isocitrate and nitroisocitrate bound have been solved and refined to *R* factors of 0.179 and 0.161, respectively, for all observed data in the range 8.0–2.1 Å. Porcine heart enzyme was used for determining the structure with isocitrate bound. The presence of isocitrate in the crystals was corroborated by Mössbauer spectroscopy. Bovine heart enzyme was used for determining the structure with the reaction intermediate analogue nitroisocitrate bound. The inhibitor binds to the enzyme in a manner virtually identical to that of isocitrate. Both compounds bind to the unique Fe atom of the [4Fe–4S] cluster via a hydroxyl oxygen and one carboxyl oxygen. A H_2O molecule is also bound, making Fe six-coordinate. The unique Fe is pulled away ~0.2 Å from the corner of the cubane compared to the position it would occupy in a symmetrically ligated [4Fe–4S] cluster. At least 23 residues from all four domains of aconitase contribute to the active site. These residues participate in substrate recognition (Arg447, Arg452, Arg580, Arg644, Gln72, Ser166, Ser643), cluster ligation and interaction (Cys358, Cys421, Cys424, Asn258, Asn446), and hydrogen bonds supporting active site side chains (Ala74, Asp568, Ser571, Thr567). Residues implicated in catalysis are Ser642 and three histidine–carboxylate pairs (Asp100–His101, Asp165–His147, Glu262–His167). The base necessary for proton abstraction from Cβ of isocitrate appears to be Ser642; the Oγ atom is proximal to the calculated hydrogen position, while the environment of Oγ suggests stabilization of an alkoxide (an oxyanion hole formed by the amide and side chain of Arg644). The histidine–carboxylate pairs appear to be required for proton transfer reactions involving two oxygens bound to Fe, one derived from solvent (bound H_2O) and one derived from substrate hydroxyl. Each oxygen is in contact with a histidine, and both are in contact with the side chain of Asp165, which bridges the two sites on the six-coordinate Fe.

Aconitase [citrate (isocitrate) hydrolyase, EC 4.2.1.3] employs a [4Fe–4S] cluster to catalyze the stereospecific dehydration–rehydration of citrate to isocitrate via *cis*-aconitase in the second and third steps of the Krebs cycle (Scheme I). The enzyme has been the subject of biochemical, spectroscopic, and kinetic experiments for over 40 years [for reviews, see Beinert and Kennedy (1989), Glusker (1971), Walsh (1979), Beinert and Thomson (1983), Emptage (1988), Beinert (1990), and Switzer (1989)]. The mechanism is of interest because of the involvement of Fe, resident in an Fe–S cluster, and because of the stereoselectivity of the reactions catalyzed. Aconitase is the best studied example of a growing class of enzymes which employ Fe–S clusters in nonredox functions as, e.g., (de)hydratases. Aconitase has also served as an excellent system for studying Fe–S cluster substitutions, rearrangements, and assembly in vitro (Beinert & Kennedy, 1989).

Key features of aconitase structure and function are activation by interconversion of a [3Fe–4S] to a [4Fe–4S] cluster (Beinert et al., 1983; Kennedy et al., 1983; Kent et al., 1982), direct involvement of the Fe atom inserted, termed Fe_a, in binding substrate (Emptage et al., 1983; Kent et al., 1985; Werst et al., 1990a,b), coordination of substrate to Fe_a via one carboxyl oxygen (α-carboxyl for isocitrate, β-carboxyl for citrate, α or β for *cis*-aconitate) simultaneously with substrate hydroxyl and H_2O from solvent (Telser et al., 1986; Kennedy et al., 1987), exchange of hydroxyl oxygen with solvent (Telser et al., 1986), and retention on the enzyme of the proton abstracted from Cα of citrate/Cβ of isocitrate during early turnover (Rose & O'Connell, 1966). The transition state in forming *cis*-aconitate from either citrate or isocitrate is expected to be a carbanion on the basis of inhibition by nitronate analogues (Schloss et al., 1980). The kinetic mechanism requires product displacement by substrate; citrate and isocitrate bind by flipping over about the Cα–Cβ bond, requiring two binding modes for the "acetyl arm" (Cγ carboxyl) as well as for the intermediate product *cis*-aconitate (Schloss et al., 1984). There are at least two catalytic groups on the enzyme, one for abstracting a proton and one for protonating substrate hydroxyl to eliminate water (Schloss et al., 1984). Further, the Fe–S cluster facilitates electron shifts, as the electron density on Fe_a changes upon binding citrate or isocitrate (Kent et al., 1985; Emptage et al., 1983). The role of the metal in hydration of the double bond of *cis*-aconitate is supported by reactivity of a Co model compound (Gahan et al., 1985).

In eukaryotic organisms, there is dual localization of aconitase in mitochondria and the cytosol (Switzer, 1989). The primary sequence of the pig heart mitochondrial enzyme has

Scheme I: Aconitase Reactions

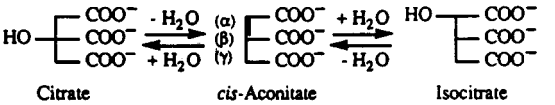

[†] This research was supported by NIH Grants GM-36325 to C.D.S. and GM34812 to H.B. In recognition of his contributions to the chemistry of sulfur compounds of biological relevance, we dedicate this paper to Professor Doriano Cavallini of Rome on the occasion of his 75th birthday.

[‡] Coordinates have been deposited with the Brookhaven Protein Data Bank [accession numbers 7ACN (isocitrate) and 8ACN (nitroisocitrate)].

* Author to whom correspondence should be addressed.

[§] The Scripps Research Institute.

[∥] Medical College of Wisconsin.

0006-2960/92/0431-2735$03.00/0

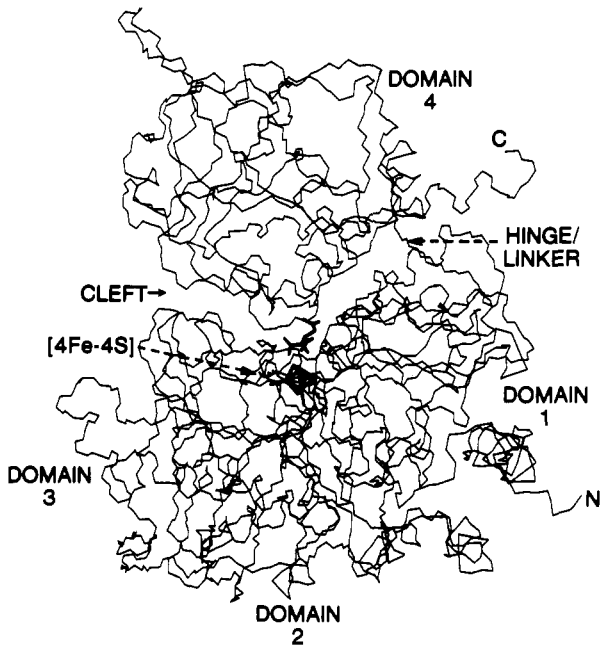

FIGURE 1: Polypeptide fold of porcine mitochondrial aconitase with the [4Fe–4S] cluster and isocitrate bound (heavy lines). N, Cα, and C atoms of the protein are shown.

been deduced from cDNA (754 amino acids, M_r 83 000) (Zheng et al., 1990). The sequences of eight cysteinyl–tryptic peptides from beef heart mitochondrial aconitase (Plank & Howard, 1988) show only three differences over 194 amino acids in comparison to the pig heart protein. The yeast enzyme is also highly homologous (Gangloff et al., 1990), where all insertions, deletions, and substitutions are compatible with the three-dimensional structure.

Recently, it has been recognized that cytosolic aconitase may be one and the same as the iron responsive element binding protein (IRE-BP) (Rouault et al., 1990, 1991). The iron-regulatory element (IRE) is an RNA stem–loop structure in the 5′ untranslated region (UTR) of ferritin mRNA (Haile et al., 1989) and the 3′ UTR of transferrin receptor mRNA (Casey et al., 1988; Koeller et al., 1989). The interaction of the two mRNAs with IRE-BP is an example of translational regulation of gene expression (Klausner & Harford, 1989). The fact that an aconitase-like protein (enzyme) binds reversibly to an RNA stem–loop structure raises the possibility that an aspect of aconitase Fe–S cluster chemistry is involved in sensing intracellular Fe concentrations and may act as a molecular switch. Eighteen residues observed in the active site of aconitase in the available crystal structures are conserved in the IRE-BP. The high degree of homology between aconitase and IRE-BP suggests that the IRE-BP is an enzyme, performing a reversible reaction which has underlying mechanistic similarity to that of aconitase (Kaptain et al., 1991).

Two crystal structures of pig heart mitochondrial aconitase have been solved: the inactive [3Fe–4S] cluster containing enzyme refined at 2.0-Å resolution (Robbins & Stout, 1989a) and the activated [4Fe–4S] cluster containing enzyme refined at 2.5-Å resolution (Robbins & Stout, 1989b). The molecule is folded into four domains: the first three are closely associated about the Fe–S cluster; the fourth is attached by an extended linker peptide creating an extensive cleft (Figure 1). The [3Fe–4S] cluster is coordinated by cysteines 358, 421, and 424. In the activated protein, the fourth Fe (Fe_a) is inserted into the corner of the [4Fe–4S] cubane structure; the fourth ligand of this Fe is a solvent molecule modeled as water or hydroxyl in the refinement. ENDOR experiments have shown that in the substrate-free enzyme this solvent molecule is a hydroxyl ion; upon binding substrate the hydroxyl is protonated to form water (Werst et al., 1990a).

In both of the available crystal structures, a sulfate ion was observed in the active site in place of tricarballylate, a weakly binding inhibitor used in crystallization. In this paper, we report a new crystal form of aconitase which accommodates substrates and inhibitors. Further, we report the refined crystal structures of the pig heart enzyme complexed to isocitrate and the beef heart enzyme complexed with nitroisocitrate, a tight binding inhibitor (Schloss et al., 1980). [In nitroisocitrate the β-carboxyl is replaced with a NO_2 group (see Scheme I above).] While these structures do not allow us to propose a complete mechanism, they do provide detailed information concerning critical aspects of the catalytic mechanism. In particular, such aspects are the nature of the base which abstracts a proton from Cβ of isocitrate and the hydrogen-bonding network involved in protonation of substrate hydroxyl and Fe-bound hydroxyl.

Experimental Procedures

Materials. Bovine heart mitochondrial aconitase was prepared as previously described (Kennedy et al., 1983). Porcine heart mitochondrial aconitase was prepared and provided by D. Aul and W. E. Brown as for the structure determination (Robbins & Stout, 1989a). DL-Isocitric acid (trisodium salt) hydrate and *trans*-aconitic acid were obtained from Aldrich. Tricarballylic acid and *cis*-aconitic acid were from Sigma. Sodium citrate dihydrate was purchased from Baker, and (±)-*cis*-epoxytricarballylic acid (monopotassium salt) was from Fluka. All other chemicals and reagents used were of analytical grade.

Buffers were deoxygenated on a Schlenk manifold by repeated evacuation and flushing with Ar and transferred to an anaerobic glove box (Coy Laboratory Products). Aliquots of 100 mM sodium dithionite in 100 mM Bis-Tris, pH 7.0, were added immediately prior to use to all buffers to a final concentration of 1 mM. Abbreviated designations for the buffer solutions are as follows, where (*n*) indicates the different concentrations of ammonium sulfate used in the crystallization procedure (*n* = 0, 2.2 M, 2.6 M, or saturated at room temperature): tricarb(*n*) buffer = *n* M ammonium sulfate in 0.015 M or 0.1 M tricarballylic acid, 0.25 M Bis-Tris·HCl, and 0.35 M NaCl, pH 7.0; cis(*n*) buffer = *n* M ammonium sulfate in 0.1 M *cis*-aconitate, 0.25 M Bis-Tris·HCl, and 0.35 M NaCl, pH 7.0; trans(*n*) buffer = *n* M ammonium sulfate in 0.1 M *trans*-aconitate, 0.25 M Bis-Tris·HCl, and 0.35 M NaCl, pH 7.0; citrate(*n*) buffer = *n* M ammonium sulfate in 0.1 M sodium citrate, 0.25 M Bis-Tris·HCl, and 0.35 M NaCl, pH 7.0; epoxy(*n*) buffer = *n* M ammonium sulfate in 0.1 M epoxytricarballylic acid, 0.25 M Bis-Tris·HCl, and 0.35 M NaCl, pH 7.0; isocitrate(*n*) buffer = *n* M ammonium sulfate in 0.1 M isocitrate, 0.25 M Bis-Tris·HCl, and 0.35 M NaCl, pH 7.0.

Porcine heart aconitase samples were diluted 3-fold with a buffer of 15 mM tricarballylate and 60 mM Tris·HCl, pH 7.8, and concentrated under N_2 using an Amicon cell concentrator with a YM30 membrane to remove sucrose and ampholytes present from the purification procedure. The procedure was repeated twice, and the protein was concentrated to 17 mg/mL. The protein solution was centrifuged, put under Ar, and transferred into the glove box. The enzyme was activated by adding aliquots of 100 mM sodium dithionite in 100 mM Bis-Tris, pH 7.0, and 100 mM ferrous ammonium sulfate to final concentrations of 2 mM each. Activation was accompanied by an immediate color change of the solution from brown to pale yellow. Bovine heart aconitase was pro-

Table I: Crystallization Experiments with Porcine and Bovine Aconitase[a]

protein	substrate or inhibitor (mM)[b]	seed crystals[c]	space group	comments[d]
porcine heart aconitase	TC (15)	O (ph)	$P2_12_12$	single crystals
	TC (15)	M (ph)	$P2_12_12$	showers of small crystals, appear to be orthorhombic
	TC (15)	M (bh)	$P2_12_12$	single crystals
	TC (75)	O (ph)	$P2_12_12$	showers of small crystals, appear to be orthorhombic
	TC (75)	M (bh)	$P2_12_12$	showers of small crystals, appear to be orthorhombic
	C (75)	O (ph)	$B2$	single crystals, tendency to twin
	C (75)	M (ph)	$B2$	single crystals, tendency to twin
	C (75)	M (bh)	$B2$	single crystals
	I (75)	O (ph)	$B2$	low yield of single crystals
	I (75)	M (ph)	$B2$	tendency to twin
	A (75)	O (ph)	$B2$	single crystals
	A (75)	M (ph)	$B2$	tendency to twin
	A (75)	M (bh)	$B2$	single crystals
	ET (75)	O (ph)	seeds crack	no crystals
	ET (75)	M (ph)	$B2$	single crystals, tendency to twin
	TA (75)	O (ph)	seeds crack	no crystals
	TA (75)	M (ph)	$B2$	tendency to twin
	TA (75)	M (bh)	$B2$	single crystals
bovine heart aconitase	TC (15)	O (ph)	$B2$	small crystals, appear to be monoclinic
	TC (15)	M (bh)	$B2$	single crystals
	C (75)	O (ph)	$B2$	single crystals
	C (75)	M (bh)	$B2$	single crystals
	TA (75)	M (bh)	$B2$	single crystals
	NI (0.33)[e]	M (bh)	$B2$	single crystals

[a] All experiments were done anaerobically. See Experimental Procedures for details. [b] Abbreviations: TC, tricarballylate; C, citrate; I, isocitrate; A, *cis*-aconitate; ET, epoxytricarballylate; TA, *trans*-aconitate; NI, nitroisocitrate. Concentrations given are for the crystallization droplets after mixing all solutions. [c] Abbreviations: O, orthorhombic, space group $P2_12_12$; M, monoclinic, space group $B2$; ph, porcine heart; bh, bovine heart. [d] All occurrences of single crystals were established with precession photographs. [e] Protein in 1 mM nitroisocitrate, 60 mM Tris·HCl, pH 7.8, was mixed in the droplet with 0.015 M tricarb(saturated) buffer.

vided as activated enzyme, 17 mg/mL, in 15 mM tricarballylate and 60 mM Tris·HCl, pH 7.8, in either 20 mM citrate, 1 mM nitroisocitrate, or in the absence of added substrates or inhibitors. The citrate-complexed enzyme was activated with ^{57}Fe. Activating agents were removed by passing the enzyme through a gel column.

Crystallization. Aconitase–substrate and aconitase–inhibitor solutions were prepared by mixing four volumes of activated 17 mg/mL protein solutions with one volume of the standard buffer solutions in the absence of ammonium sulfate, e.g., cis(0). All of these and subsequent operations were performed anaerobically at room temperature in the glove box with an atmosphere of 96% N_2, 4% H_2, and $\leq$1 ppm O_2. Aconitase–substrate and aconitase–inhibitor solutions were allowed to stand 1 h prior to exposure to ammonium sulfate in the crystallization procedure.

The crystallization procedure followed that established for growing orthorhombic crystals of pig heart aconitase (Robbins et al., 1982; Robbins & Stout, 1985) except that it was done anaerobically. The glove box was equipped with a microscope for selection of seed crystals. The procedure uses the vapor diffusion method and hanging drops. Drops were prepared by mixing 12 μL of the aconitase–substrate or aconitase–inhibitor solutions, e.g., cis(0) above, with 18 μL of the corresponding buffers in saturated ammonium sulfate, e.g., cis(saturated) buffer. Drops were placed onto a silicon grease treated cover slip and microseeded. Seed crystals were washed and incubated in the corresponding buffer solution in 2.6 M ammonium sulfate, e.g., cis(2.6 M) buffer, and transferred in 1.5 μL of this stabilizing solution to the drop. Seed crystals were usually smaller than 0.05 mm in maximum dimension and were harvested from other drops anaerobically or from drops of aerobically grown orthorhombic crystals of porcine aconitase. In the latter case, the seed crystals were transferred into the glove box under Ar in a degassed stabilizing solution, e.g., cis(2.6 M) buffer. Seeded droplets were inverted over 1-mL reservoirs of 2.2 M ammonium sulfate in the corresponding buffer, e.g., cis(2.2 M). For data collection, crystals were transferred and washed with a stabilizing solution of the appropriate buffer in 2.8 M ammonium sulfate, e.g., cis(2.8 M). Crystals were mounted anaerobically in thin-walled glass capillaries, which were sealed with epoxy resin.

The results of seeding and crystallization experiments with porcine and bovine heart mitochondrial aconitase are summarized in Table I. Large single crystals of pig heart aconitase in the orthorhombic space group $P2_12_12$ invariably cracked and disintegrated when soaked anaerobically in substrate or inhibitor solutions. However, these crystals as seeds induced crystallization of activated enzyme–substrate and enzyme–inhibitor crystals in a new space group. Crystals were rhombohedral in appearance and grew over a period of 6 weeks to 3 months to reach maximum dimensions of 1.0 × 1.0 × 0.2 mm. Precession photography established that the crystals are monoclinic with the symmetry of space group $B2$. The unit cell dimensions are a = 185.5, b = 72.0, and c = 73.0 Å and γ = 77.7°. For one 83 000 dalton molecule in the asymmetric unit, the volume per unit mass is 2.9 Å^3/dalton (57% solvent content), within the range found to be typical of protein crystals (Matthews, 1968). The $B2$ space group was chosen for comparison to the $P2_12_12$ unit cell, which has a = 173.6, b = 72.0, and c = 72.7 Å and a 2-fold axis parallel to c as in $B2$.

Once monoclinic crystals were obtained, they were used as seeds to induce further crystallization of single monoclinic crystals (Table I). It was also possible to cross-seed between pig and beef heart enzymes (Table I). Precession photographs showed that the crystals were isomorphous regardless of the species of enzyme used for crystallization or species of enzyme

Table II: Data Collection with Monoclinic Aconitase Crystals[a]

structure	isocitrate	nitroisocitrate	test	Pt derivative
source	pig heart	beef heart	pig heart	pig heart
compound used in crystallization	*cis*-aconitate	nitroisocitrate	citrate	*cis*-aconitate
compound present in active site	isocitrate	nitroisocitrate	isocitrate	(isocitrate)
number of crystals	4	2	1	1
maximum resolution (Å)	2.10	2.05	2.66	3.6
total observations	435 630	268 600	72 828	108 074
unique reflections	49 211	50 902	17 023	10 178
possible reflections	54 710	58 710	26 829	11 143
completeness	89.9%	86.7%	63.5%	91.3%
resolution of last shell of data (Å)	2.24–2.10	2.18–2.05	2.83–2.66	3.81–3.60
completeness of last shell of data	54.7%	49.8%	20.2%	55.1%
average $I/\sigma(I)$ for all data	18.9	26.4	26.5	29.3
average $I/\sigma(I)$ in last shell	3.8	5.9	5.5	15.8
$R_{symm}(F)$ for all data	6.83%	5.11%	6.43%	5.14%

[a] Data summarized are for all observations of intensities or $|F|$ greater than 0.0σ.

used for the seed crystal. The pig heart enzyme crystallized only in the $P2_12_12$ space group when tricarballylate was present either at low or high concentration, whereas the beef heart enzyme yielded monoclinic crystals with this inhibitor. All other experiments yielded the $B2$ space group (Table I).

Data Collection. Crystals obtained with three of the compounds listed in Table I have been used for data collection: pig heart enzyme grown in the presence *cis*-aconitase and citrate and beef heart enzyme grown in the presence of nitroisocitrate. An explanation for the presence of isocitrate in the *cis*-aconitate and citrate grown crystals is given under Results. *cis*-Aconitate grown crystals were also used for the Pt derivative data collection. In this case, crystals were soaked anaerobically in cis(2.9 M) buffer containing 15 mM K_2PtCl_4 for 3 days.

X-ray diffraction data were collected using a GX-21 rotating anode generator with a 0.2-mm focal spot and Ni-filtered Cu Kα radiation. Data were recorded with a Xentronics area detector and processed with the XENGEN suite of programs (Howard et al., 1985) implemented on Unix computers at Scripps. The detector was equipped with a helium cone and crystals were maintained at 18 °C. Data were collected in ω sweeps with steps of 0.25°/frame using alternate 2θ settings of 25° and 0° to cover high- and low-resolution ranges. The detector was set at 15 cm from the crystal and 2θ 0° runs were used for autoindexing prior to indexing 2θ 25° runs at the same ϕ,ω settings. Regions of the crystals were exposed 5–7 days, and then the crystals were translated in the beam to a fresh region, allowing two or three regions per crystal to be collected. Crystals were mounted in two orthogonal orientations to allow coverage of all unique reflections. Only those reflections occluded by the beamstop were omitted from the low-resolution data. Data are summarized in Table II.

Structure Determination. To determine the structure of the complexes in the monoclinic crystal form, we used the molecular replacement method and confirmed the result with the Pt derivative and anomalous scattering from the Fe–S cluster. The first structure solved was of the pig heart enzyme grown from *cis*-aconitate (isocitrate structure in Table II). The search model was the 2.1-Å refined structure of inactive ([3Fe–4S] cluster) pig heart aconitase with sulfate bound in the $P2_12_12$ space group (Robbins & Stout, 1989a). The Fe–S cluster, sulfate, and water molecules were deleted from the model. Using the MERLOT program (Fitzgerald, 1988) in space group $B2$, all atoms of residues 2–754, and 8.0–3.5-Å resolution data, the Crowther rotation function gave a peak at 17.0σ at $\alpha = 0°$, $\beta = 90°$, $\gamma = 0°$. This orientation was refined with the Lattman rotation function ($\alpha = 0°$, $\beta = 89.9°$, $\gamma = 0.2°$) and used for a translation search, which yielded a 23.4σ peak at $x = 0.13$, $y = 0.46$, $z = 0$. The rotation–translation solution was refined with the RMIN program (Fitzgerald, 1988). The molecule was then broken into two fragments, residues 2–520 and 521–754, and the fragment orientations further refined with the program INTREF (Yeates & Rini, 1990), resulting in shifts in the range –0.13°–0.97°. The fragment of residue 2–520 was then fixed and the fragment of 521–754 refined relative to it, resulting in further shifts of –0.38–0.1° and –0.5–0.12 Å. This refined model was input to the translation search in XPLOR (Brünger et al., 1989), which yielded the same solution as obtained with MERLOT.

Table III: Pt Derivative of Monoclinic Aconitase

site[a]	x	y	z	nearest protein atoms	distance (Å)
1	26.1 Å	66.1 Å	75.4 Å	His692 NE2[b]	4.9
2	69.2	61.9	106.3	His9 NE2	3.9
3	15.0	44.0	77.7	His306 NE2[b]	4.7
				Lys231 NZ[c]	4.8
				Glu636 OE2[c]	5.7
4	50.5	64.5	86.8	His626 NE2	3.2

[a] Coordinates are with respect to an orthogonal cell with x along the a, y along b^*, and z along c. [b] Histidine residue also ligated by K_2PtCl_4 in space group $P2_12_12$ (Robbins & Stout, 1989a). [c] Residue on a symmetry-related molecule.

The oriented, translated, two-fragment model was used for rigid-body refinement in XPLOR against 8–4-Å data. The initial R factor was 0.331, and the refinement converged at 0.313. A series of rigid-body refinements was then done at increasing resolution (3.5, 3.2, 3.0 Å) converging at R of 0.224. A $2|F_o| - |F_c|$ map using data in the range 20–3-Å resolution showed clear density for the Fe–S cluster, which had not been included in the model, as well as density for substrate and indication of side-chain rearrangements in the active site.

In addition to the R factor and new electron density features, the validity of the molecular replacement solution was supported by the anomalous difference Patterson map calculated with data in the resolution range 20–5 Å from *cis*-aconitate grown pig heart aconitase crystals. The map showed a single large peak 2.5 times the noise level in the $w = 0$ Harker section at $u = 0.31$, $v = 0.87$. The vector calculated from the model for the center of gravity of the Fe–S cluster is at $u = 0.31$, $v = 0.86$. The molecular replacement solution is further supported by the Pt derivative data (Table II). A difference Fourier map using data in the resolution range 20–4 Å showed four strong peaks for Pt sites, each near putative ligand residues in the 3.0-Å resolution refined monoclinic structure (Table III). All sites occurred on the surface of the protein molecule. The 5-Å resolution anomalous difference Patterson map for the Pt data also showed the Fe–S vector at $u = 0.31$,

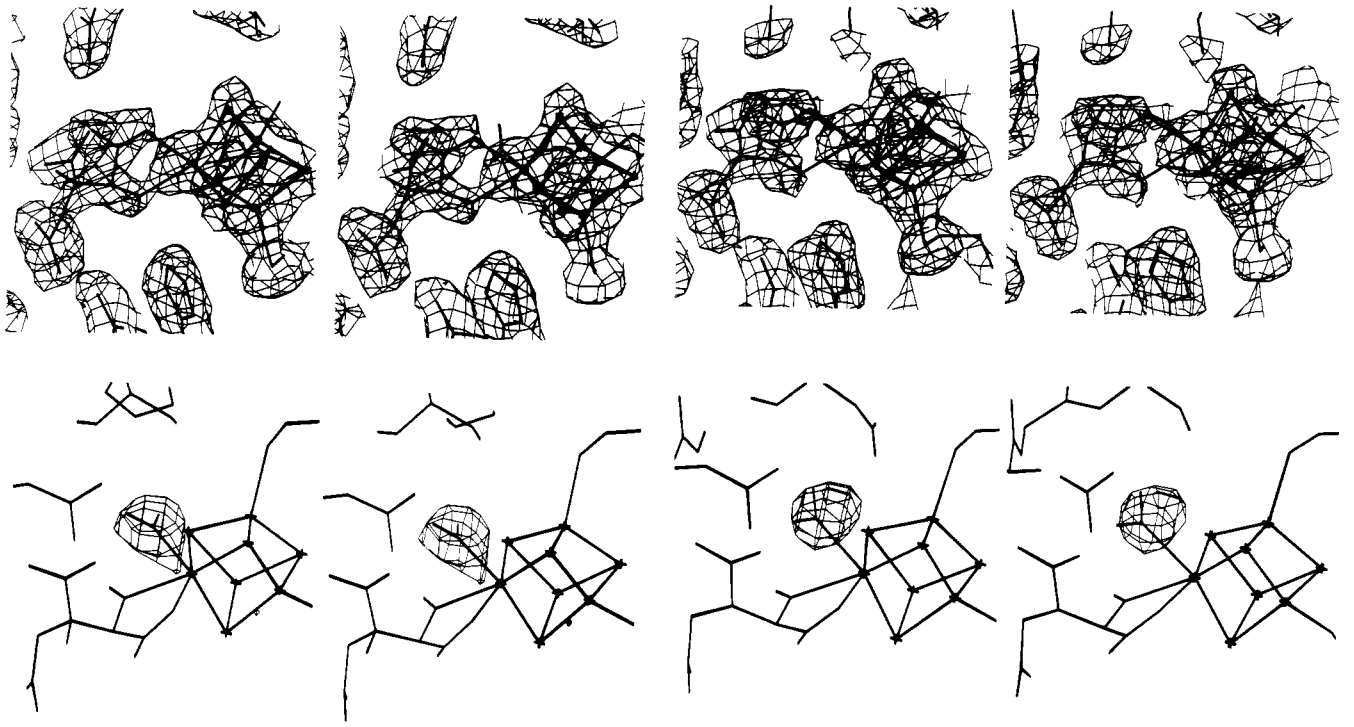

FIGURE 2: Electron density maps in stereo for mitochondrial aconitase structures calculated with data in the range 20–2.1-Å resolution. (a, top left) $2|F_o| - |F_c|$ map showing isocitrate bound to the [4Fe–4S] cluster. (b, bottom left) $|F_o - F_c|$ map for H_2O bound to sixth coordination site of a unique Fe of the [4Fe–4S] cluster (Fe4, Fe_a) in the structure of the porcine enzyme with isocitrate bound. Note in panels a and b that hydrogens are included in the model for H_2O and for isocitrate on the hydroxyl oxygen and on Cβ atom. (c, top right) Same as in panel a for nitroisocitrate bound to the [4Fe–4S] cluster. (d, bottom right) Same as in panel b for H_2O on Fe4 in the structure of the bovine enzyme with nitroisocitrate bound. Hydrogen is included in the model for H_2O and for the inhibitor on the hydroxyl oxygen but not on the Cβ atom (see text). Panels a and c are contoured at 0.13 of the maximum density, which is on the Fe–S cluster, and panels b and d are contoured at 0.3 of the maximum density, which is on the water molecule shown. Note that in panel a some bonds of atoms not in [4Fe–4S] and isocitrate are truncated by clipping planes used to make the figure; similarly in panel d some bonds in side chains adjacent to the bound water are truncated.

$v = 0.87$, $w = 0$ at 2 times the background.

Refinement. Refinement of the monoclinic structure was extended to 2.1 Å using data from the *cis*-aconitate grown pig heart aconitase crystals (Table II). Positional refinement with XPLOR was carried out in 13 ranges of increasing resolution starting at 8.0–4.0 Å and finishing at 8.0–2.1 Å with an R factor of 0.231 for all observed data. Water molecules were included in the model, refined, and edited in $2|F_o| - |F_c|$ maps calculated with all data in the resolution range 20–2.1 Å in three passes through the structure, which included checking and adjusting the conformation of all the side chains. Isotropic B factors were refined for all atoms, resulting in R of 0.193. The entire model was then subjected to simulated annealing refinement (Brünger et al., 1989) starting at 4000 K and cooling in 25 K steps to 300 K; following positional and B-factor refinement, the R was 0.188. The water structure was edited again and B factors were refined, yielding R of 0.184.

Up to this point, the electron density for the substrate had not been modeled. A 20–2.1-Å resolution $2|F_o| - |F_c|$ map showed clear density for isocitrate (Figure 2a) with the correct 2*R*,3*S* stereochemistry (Carrell et al., 1970). The initial model was obtained from a Monte-Carlo search algorithm as part of a systematic search of binding modes of aconitase substrates (Goodsell & Olson, 1990) and required only minor adjustment. For refinement, an idealized model for isocitrate was constructed using distances and angles from a small molecule crystal structure (Carrell et al., 1970), XPLOR energy constraints for C–C, C–O, C–H, and O–H bonds and angles, and charges for carboxyl groups (pH of crystals 7.0, pK_as of isocitrate 3.3, 4.7, and 6.4). Hydrogens on the substrate Cβ and hydroxyl oxygen were included in the model as an aid for interpretation of interactions with the protein. Covalent bonds were defined for substrate OA2 and OHA to Fe4 of the cluster, as for the cysteine Sγ ligands to the other Fe atoms of the cluster. Positional refinement with the substrate included yielded R of 0.180.

A difference Fourier map using data in the range 20–2.1 Å revealed a large peak adjacent to the Fe–S cluster (Figure 2b). This peak was modeled as a H_2O molecule on the basis of the ENDOR data for substrate-bound aconitase (Werst et al., 1990a). Again, hydrogens were included as an aid in interpretation. The H_2O molecule was included as part of Fe–S cluster constrained to the position of the maximum in the difference Fourier peak. Positional and B-factor refinement yielded R of 0.179 for all observed reflections with $|F_o| > 0$ in the range 8.0–2.1 Å.

The model has 6174 non-hydrogen atoms (5815 protein, 9 Fe–S cluster, 13 substrate, and 337 water). The rms deviations from ideality of bonds and angles are 0.015 Å and 3.09°, respectively. The Ramachandran plot is shown in Figure 3, and the Luzzati plot is shown in Figure 4a. The overall B factor for the structure is 21.5 Å^2; the average B factors of [4Fe–4S](H_2O) and isocitrate are 14.3 and 15.7 Å^2, respectively. The following residues have B factors on their Cα atoms exceeding 40 Å^2 and are in weak density: 1–2, 342–343, 434–435, 490–492, 498, 501, 509, 514–515, 522–528, 718–721, and 751–754. These regions are exposed loops at the "corners" of the molecule, the N- and C-termini, or part of the extended chain leading to and including the hinge/linker region. Of 337 water molecules in the model, 126 have B factors exceeding 40 Å^2 (maximum 62 Å^2).

The refined pig heart aconitase structure containing isocitrate was used as a starting point for refinement against data from the nitroisocitrate complexed beef heart enzyme (Table

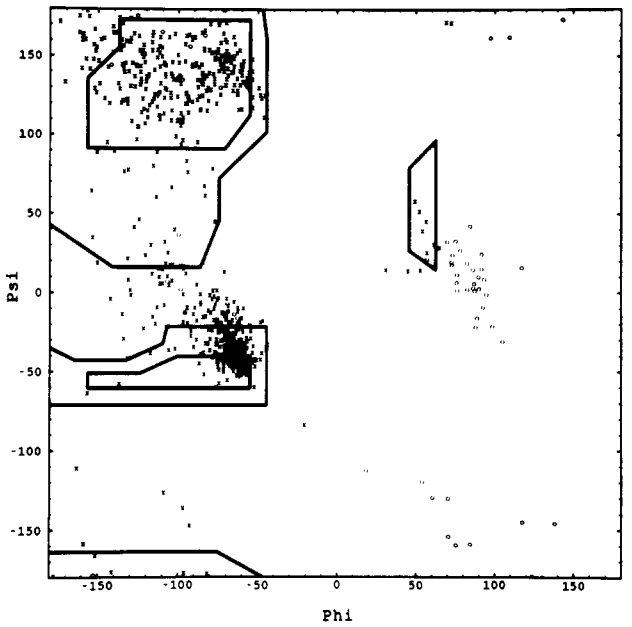

FIGURE 3: Ramachandran plot for refined aconitase structure with isocitrate bound. Glycines are plotted as circles; all other residues are plotted as crosses. The plot for the structure with nitroisocitrate bound is virtually identical.

II). Only the isocitrate and H_2O bound to the [4Fe–4S] cluster were omitted from the coordinates. Rigid-body refinement with XPLOR for data in the resolution range 8.0–4.0 Å gave R of 0.171. Positional and B-factor refinement in nine ranges of increasing resolution resulted in R of 0.166 for all data in the resolution range 8.0–2.1 Å. At this stage, the water structure was edited and updated, and all side-chain conformations were checked and adjusted if necessary, especially those with high B factors. This process included substituting the known beef heart sequence changes (P303 → S, V310 → L, K712 → T) (Plank & Howard, 1988); all three beef heart residues were clear in a $2|F_o| - |F_c|$ map, using data of 20–2.1 Å resolution. In this process, three additional residues for which there are no beef heart sequence data, but which did have clear density, were substituted: I597 → S(A), H653 → F(F), and H692 → N(N). The residues in parentheses are from the yeast aconitase sequence (Gangloff et al., 1990). All of these sequence changes were for surface residues; none of the residues near the active site were changed or appeared to be different than in the pig heart enzyme. Positional and B-factor refinement gave R of 0.163.

This model was used to calculate $2|F_o| - |F_c|$ and $|F_o| - |F_c|$ maps with data in the range 20–2.1 Å for modeling the nitroisocitrate (Figure 2c) and bound water (Figure 2d). These atoms were included in the refinement in a manner analogous to the isocitrate refinement, except that the hydrogen on Cβ was omitted. The Cβ atom was not constrained to be trigonal, however. Following positional and B-factor refinement, the R is 0.161 for all reflections with $|F_o| > 0$ in the range 8.0–2.1 Å.

The structure of the nitroisocitrate complex of the enzyme consists of 6154 atoms (5812 protein, 9 Fe–S cluster, 13 inhibitor, and 320 water). The rms deviations from ideality of bonds and angles are 0.015 Å and 3.03°, respectively. The Luzzati plot is shown in Figure 4b. The overall B factor for the structure is 17.7 Å^2; the average B factors of [4Fe–4S](H_2O) and nitroisocitrate are 10.9 and 15.7 Å^2, respectively. Thus, even though the structure as a whole has a lower B factor than the structure with bound substrate, the B factors for substrate and inhibitor are the same. Only 22 residues have

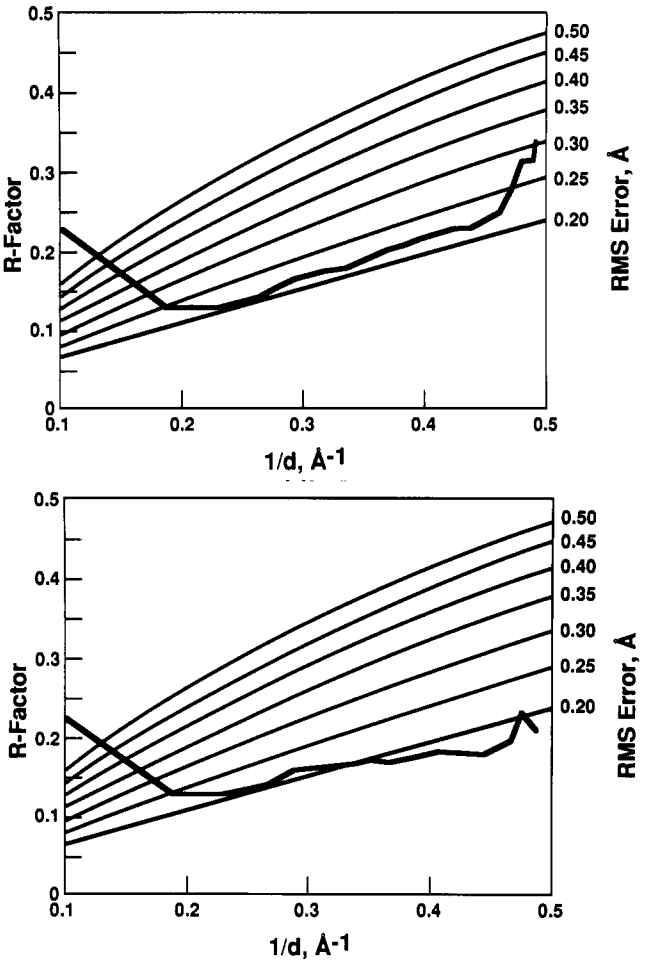

FIGURE 4: Luzzati plots for refined aconitase structures with isocitrate (a, top) and nitroisocitrate (b, bottom) bound. Curves are calculated with all data in the resolution range 10–2.0 Å for rms coordinate errors of 0.20–0.50 Å.

Cα with $B > 40$ Å^2 vs 29 in the enzyme with isocitrate bound, but all are localized within the same regions. A total of 80 of the 320 water molecules have B factors exceeding 40 Å^2 (maximum 62 Å^2).

RESULTS

Stereoviews of the active site region of the enzyme with isocitrate and nitroisocitrate bound are shown in Figure 5, panels a and b, respectively. All contacts of the substrate and inhibitor to aconitase are displayed in Figure 6a,b. The principal results of the structure determinations are as follows. First, the substrate and inhibitor bind to the enzyme in a virtually identical manner. Second, coordination to Fe4 (Fe_a) of the [4Fe–4S] cluster is via one carboxyl oxygen and hydroxyl oxygen, while an additional H_2O molecule binds to this Fe making it six coordinate (Figure 7a,b). This structure is in agreement with the structure deduced from spectroscopic and chemical labeling experiments (Werst et al., 1990a,b; Telser et al., 1986; Kennedy et al., 1987). Third, the base involved in the abstraction a proton from Cβ trans to the hydroxyl appears to be a deprotonated serine (alkoxide) which resides in an oxyanion hole (Figure 8). Fourth, a network of possible hydrogen bonds surrounds the substrate hydroxyl and Fe-bound H_2O (Figure 9); these would appear to be important in the mechanism for protonation/deprotonation of both oxygens. Fifth, specific contacts are made by the enzyme to each of the substrate carboxyl groups (Figures 5 and 6); these contacts account for stereoselectivity but at the same time

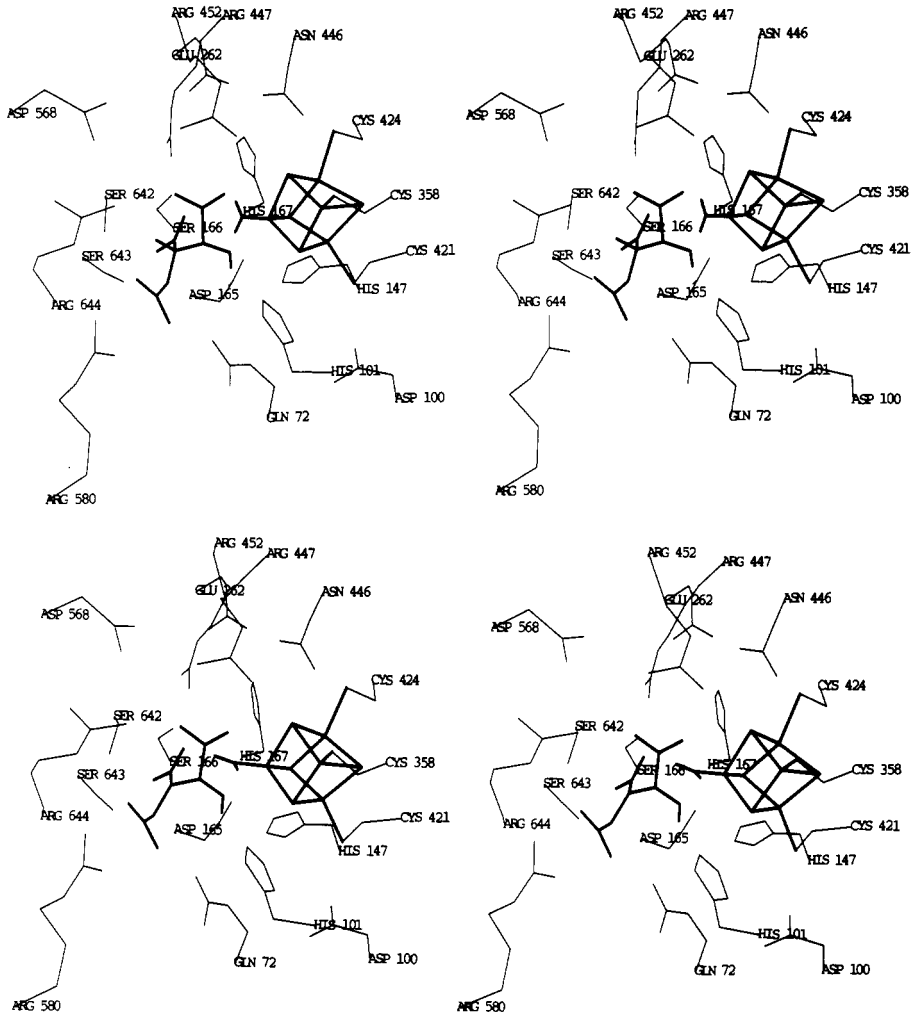

FIGURE 5: Stereoviews of the active site regions in porcine (a, top) and bovine (b, bottom) mitochondrial aconitase. The Cα atoms and side chains of 19 adjacent residues are shown. The substrate isocitrate (a) and inhibitor nitroisocitrate (b) are shown in heavy lines along with [4Fe–4S] cluster and bound H_2O with hydrogens included as in Figure 2.

are not inconsistent with an alternative positioning of the Cγ carboxyl when citrate is bound. This aspect of the structure supports the kinetic results that Cα and Cβ carboxyls together with hydroxyl of citrate and isocitrate bind by flipping over about the Cα–Cβ bond, requiring in effect a "migration" of the Cγ carboxyl moiety (Schloss et al., 1984). Interactions with the substrate are supported by a secondary network of hydrogen bonds in the active site.

Isocitrate Bound. Prior to supporting each of these conclusions with details from the crystal structures, we must first consider reasons for the observation that only isocitrate is bound in the substrate cocrystallized enzyme (*cis*-aconitate or citrate, Table II). Superposition of aconitase structures from monoclinic and orthorhombic lattices shows a conformational change of the fourth domain with respect to the rest of the molecule due to the motion in the hinge/linker region. The shifts are on the order of 1° rotations and 1-Å translations (INTREF program results above). [A detailed analysis of the conformational change and comparison of the structure in two crystal forms will be presented elsewhere.] While the changes are not large, they raise the possibility that different conformers of aconitase exist depending upon the substrate bound. In other words, one could imagine that crystallization in the monoclinic form requires trapping of only one conformer into the lattice. On the other hand, the mother liquor contains activated enzyme in the presence of excess substrate (Table I), so it is also possible that the crystals could contain an equilibrium mixture of more than one substrate.

To determine the substrate composition of the crystals, 27 mg of beef heart aconitase was activated with ^{57}Fe and crystallized in the presence of citrate using monoclinic beef heart seed crystals (Table I). Large single crystals (5.5 mg) were harvested, washed free of dissolved enzyme, and used to record the Mössbauer spectrum (M. C. Kennedy, H. Beinert, H. Lauble, C. D. Stout, B. G. Fox, and E. Münck, unpublished results). Mössbauer spectra of frozen solutions of aconitase show two distinct quadrupole doublets attributable to enzyme with bound substrate. Experiments in which the enzyme was freeze-quenched rapidly after addition of citrate or isocitrate indicated that the two species observed represent the complexes with the individual substrates (Kent et al., 1985). The Mössbauer spectrum observed with crystals, however, showed only a single quadrupole doublet, i.e., only one species of the bound form present with the parameters of the form that is dominant in the first 35 ms of mixing isocitrate with enzyme (Kent et al., 1985). Assay of the dissolved crystals showed that the enzyme had the expected specific activity. Together, these data support the interpretation of the electron density (Figure 2a) in terms of isocitrate as the only species bound to the crystalline enzyme.

The presence of a single substrate in the crystals greatly simplifies the crystallographic analysis. A detailed study to determine why only isocitrate should have been bound in the crystals will be presented elsewhere. However, to further test

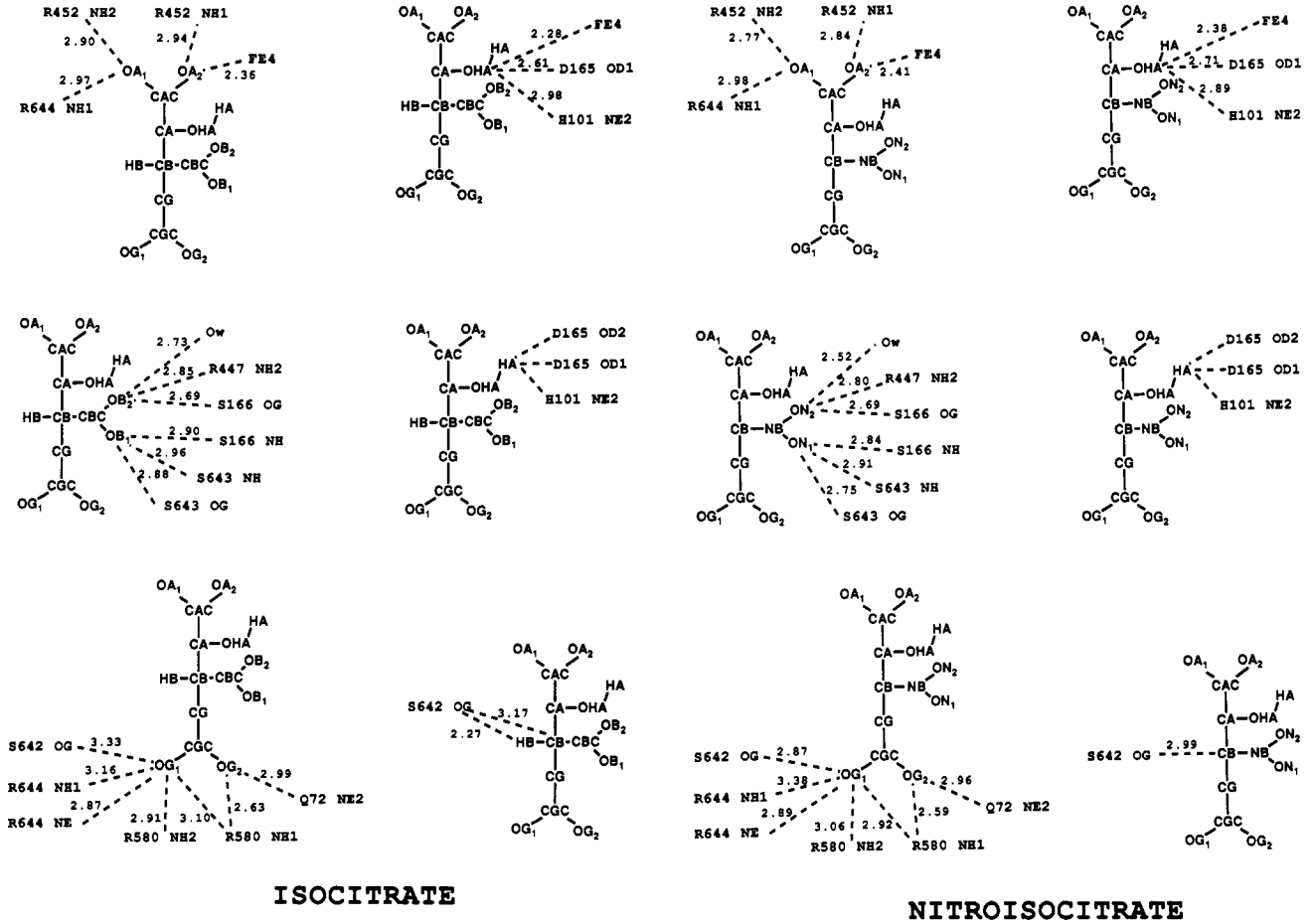

FIGURE 6: (a, left) Summary of hydrogen bonds and short contacts to isocitrate as observed in the crystal structure of porcine mitochondrial aconitase. Hydrogen bonds are indicated if the donor···acceptor distance is <3.5 Å and the angle at the possible hydrogen position is 180° ± 40°. Contacts <3.5 Å to modeled substrate hydrogens (HA and HB) are also indicated. Contacts given for HA include all possible rotomers of CA–OHA–HA; therefore, specific distances for contacts to the calculated position of HA are not given. (b, right) Summary of hydrogen bonds and short contacts to nitroisocitrate as observed in the crystal structure of bovine mitochondrial aconitase. Criteria for hydrogen bonds and contacts are as in panel a. Only the hydrogen on the hydroxyl of the inhibitor is modeled (HA).

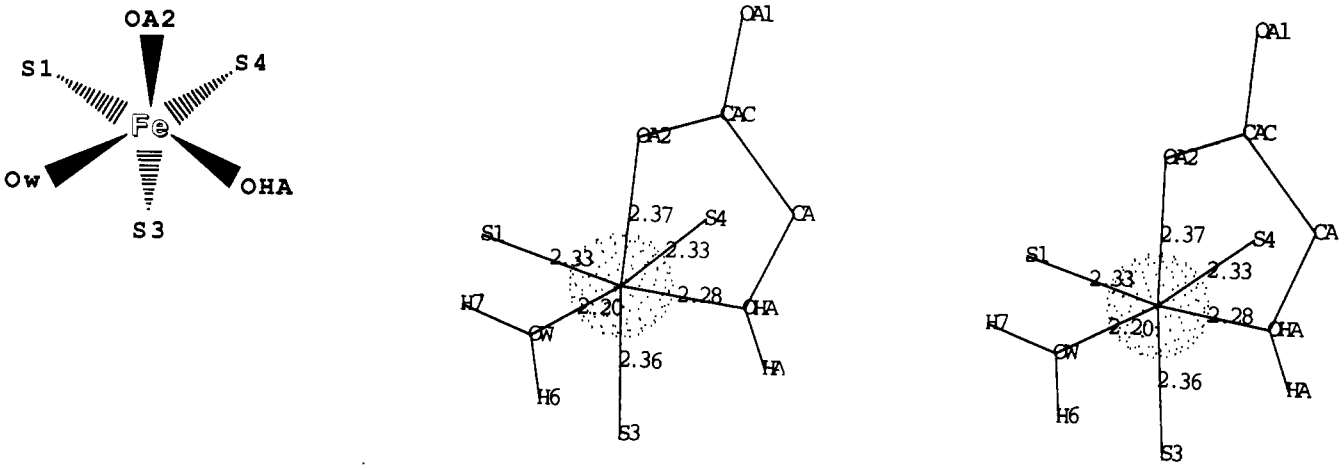

FIGURE 7: Geometry of the Fe4 (Fe_a) site in aconitase with isocitrate bound to the [4Fe–4S] cluster. (a, left) 6-fold coordination to Fe4; see Figure 6 for oxygen atom labeling; Ow is H_2O. (b, right) Stereoview of the Fe4 site with bond distances indicated.

the result, a data set was collected from a crystal grown in the presence of 75 mM citrate (Table II). A $2|F_o| - |F_c|$ map was calculated using data 20–3.0 Å and refined phases from the structure with isocitrate bound which were calculated at the stage prior to inclusion of isocitrate in the model (R 0.184, above). The map showed electron density in agreement with the refined isocitrate model. Finally, it is clear from the results of crystallization experiments (Table I) that the monoclinic lattice accommodates not only isocitrate but at least four inhibitors. Therefore, the presence of nitroisocitrate in crystals grown from the inhibitor is expected on the basis of isomorphism with crystals of the enzyme with isocitrate bound.

Comparison of Two Structures. A least-squares superposition of backbone N, Cα, C, and O atoms for all residues of the isocitrate- and nitroisocitrate-bound enzymes results in rms deviation of 0.185 Å. Using this alignment, the 22 atoms (excluding hydrogens) of the [4Fe–4S](H_2O) (isocitrate/nitroisocitrate) moieties differ by 0.283 Å on average. This is

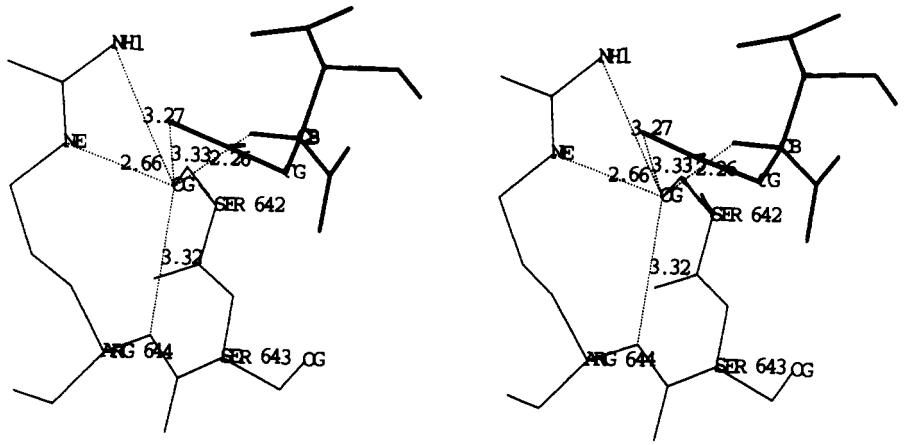

FIGURE 8: Stereoview of the oxyanion hole in aconitase. All atoms of residues SerSerArg644 are shown giving rise to contacts to OG of Ser642, the putative base in the reaction. Isocitrate is shown in heavy lines with HA and HB atoms included. Considering tetrahedral geometry at the OG atom, there are two possible hydrogen bonds from NE and amide of Arg644 as well as the short OG–HB contact. There are also two additional contacts from NH1 of Arg644 and the Cγ carboxyl of substrate.

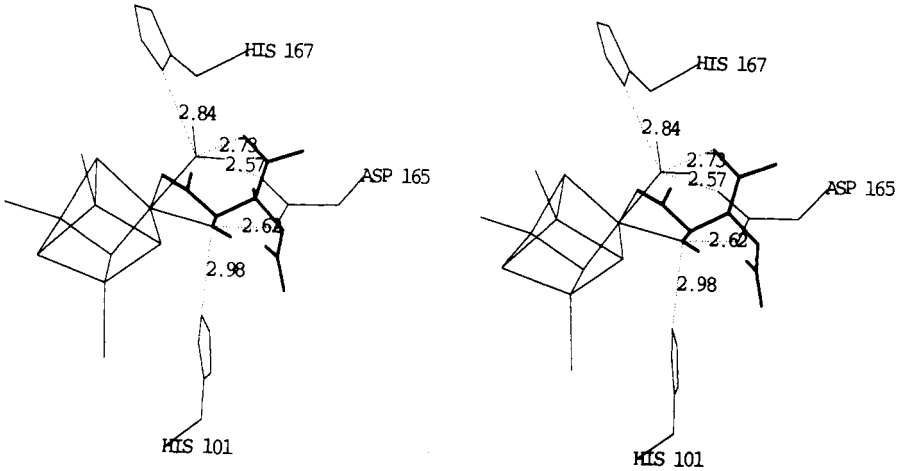

FIGURE 9: Stereoview of atoms which are part of a putative proton relay network involving two oxygen atoms bound to Fe4, one derived from substrate hydroxyl and the other from H_2O. Possible hydrogen-bond distances are indicated. However, the hydrogen positions shown are those resulting from the potential energy function used in refinement as they cannot be deduced directly from the X-ray data. Note the contact for OB2 to Fe–OH_2 (Ow) (2.73 Å) and the "cis" configuration of the two carboxyl groups.

no more than random error expected from Luzzati plots (Luzzati, 1953) for each structure (Figure 4); for isocitrate, the average error in coordinates is 0.2–0.3 Å, and for nitroisocitrate it is 0.15–0.25 Å. A potentially significant difference is at the bound H_2O molecule which is shifted toward the nitro group in the inhibitor structure (Ow contacts in Figure 6a,b). All of the active site residues have the same structure within random error, and both compounds have equivalent contacts with the enzyme (Figure 6a,b). Also, ordered water molecules trapped in the vicinity of the active site are observed at common positions in both structures. These data show that nitroisocitrate and isocitrate bind in a virtually identical manner. Nitroisocitrate is expected to bind very tightly to aconitase (Schloss et al., 1980) because, in its carbanion form, it mimics a reaction intermediate which is trigonal at Cβ and which has greater negative charge on Cβ carboxyl oxygens (aci-acid resonance form) (Schloss et al., 1980). We are of course not sure whether at the pH of the crystals (7.0) this form prevails when nitroisocitrate is bound.

Fe–S Cluster. The coordination to Fe4 (Fe_a) of the [4Fe–4S] cluster in the enzyme with isocitrate bound is depicted in Figure 7. The coordination by nitroisocitrate is virtually the same. The structure is in agreement with results from spectroscopic experiments (Kent et al., 1985; Telser et al., 1986): isocitrate binds Fe via hydroxyl and one Cα carboxyl oxygen, and a H_2O molecule is bound. On the basis of ENDOR results (Werst et al., 1990a), both protons on the H_2O have been modeled in the refinement. Distances and angles are summarized in Figure 7b and Table IV. Compared to an ideal octahedral angle (90°), the S–Fe–S angles at Fe4 are expanded by about 10°; at the same time, the average value (101°) is smaller than the 104° average angle at tetrahedrally coordinated Fe in other Fe–S clusters (Table IV). O–Fe–S angles for ligands trans to Fe4 are significantly less than 180°, reflecting the distortion required by a bidentate substrate chelate (OA2–Fe4–OHA angle 68°).

Subdividing the [4Fe–4S] cluster into the Fe4 site and a [3Fe–4S] moiety reveals an apparent distortion of the cubane in comparison to other [4Fe–4S] clusters (Table IV). Restraints used in the refinement were the same for all Fe–S distances and angles regardless of subsite. Fe–S bonds are slightly longer and Fe···Fe distances are distinctly greater at Fe4, 2.85 vs 2.65 Å, showing that Fe4 is pulled away from the corner of the [4Fe–4S] cubane. Although the difference of 0.2 Å is comparable to the estimated average error (Figure 4), difference Fourier maps calculated with Fe4 at the symmetrical position always showed positive and negative density features indicating displacement of Fe4 away from the [3Fe–4S] moiety. Consequently, S–Fe–S angles at Fe4 are compressed, compared to the [3Fe–4S] moiety. The same trends are observed in the structure of the nitroisocitrate-bound enzyme. Together, the geometrical factors show that the Fe4

Table IV: Geometry of the [4Fe–4S] Cluster in Aconitase with Isocitrate Bound and Comparison to Other [4Fe–4S] Clusters

moiety	distance/angle	no.	av	range
Fe4 site[a]	Fe4–S	3	2.34 Å	2.33–2.36 Å
	Fe4–O	3	2.27 Å	2.20–2.33 Å
	Fe4···Fe	3	2.85 Å	2.82–2.87 Å
	S···S	3	3.61 Å	3.53–3.66 Å
	S–Fe4–S	3	101°	99–102°
	O–Fe4–S (cis)	6	91°	85–98°
	O–Fe4–S (trans)	3	161°	153–167°
	O–Fe4–O	3	74°	68–79°
	Fe4–S–Fe	6	76°	75–78°
[3Fe–4S][b]	Fe–S	9	2.30 Å	2.29–2.33 Å
	Fe···Fe	3	2.65 Å	2.64–2.67 Å
	S···S	3	3.70 Å	3.66–3.73 Å
	S–Fe–S	9	106°	102–110°
	Fe–S–Fe	6	70°	69–72°
[4Fe–4S][c]	Fe–S	12	2.27 Å	2.22–2.32 Å
	Fe···Fe	6	2.74 Å	2.67–2.81 Å
	S···S	6	3.58 Å	3.49–3.65 Å
	S–Fe–S	12	104°	103–104°
	Fe–S–Fe	12	75°	74–76°
				weight
restraints[d]	Fe–S	12	2.31 Å	500 kcal/mol
	Fe···Fe	6	2.75 Å	500
	S···S	6	3.70 Å	500
	S–Fe–S	12	109°	70
	Fe–S–Fe	12	75°	70

[a] Includes S1, S3, and S4 (Figure 7). [b] Fe1, Fe2, and Fe3 ligated by Cys358, Cys424, and Cys421, respectively (Figure 5). [c] Average values for $[4Fe–4S]^{2+}$ clusters in crystal structures of two electron transfer proteins and two synthetic inorganic complexes (Carter, 1977). [d] Target values for ideal geometry of a [4Fe–4S] cluster used in refinement with XPLOR. By comparison, the weights used for C–C bonds and C–C–C angles were 450 and 70 kcal/mol, respectively.

site is pulled away 0.2 Å from the corner of the [4Fe–4S] cubane, perhaps to satisfy requirement for octahedral coordination in a tetrahedral environment (three sulfurs of [3Fe–4S]).

^{14}N and ^{1}H ENDOR data for aconitase with and without substrate bound show signals indicative of a NH···S interaction to the Fe–S cluster (Werst et al., 1990b; Houseman et al., 1992). This interaction is not affected by substrate binding to Fe_a (Fe4) and is therefore expected to involve the [3Fe–4S] moiety. The crystal structure in the absence of substrate exhibits two potential NH···S hydrogen bonds from Asn258 and Asn446 (Robbins & Stout, 1989a). Both interactions are preserved in the presence of isocitrate: the ND2 atom of Asn258 to the SG atom of Cys358 (3.28 Å, N–H···S angle 159°) and the ND2 atom of Asn446 to S1 of the cluster (3.34 Å, N–H···S angle 171°). Cys358 SG is bonded to Fe1, and S1 is bonded to Fe1, Fe2, and Fe4. Because the latter interaction involves a sulfur bonded to Fe4, the structure suggests that the Asn258–Cys358 hydrogen bond is responsible for the observed ENDOR signal.

Oxyanion Hole. The aconitase reaction requires that a proton be abstracted from Cβ of isocitrate trans to the hydroxyl (Cα of citrate); this proton is conserved on the enzyme during early turnover (Rose & O'Connell, 1966). The crystal structures suggest that the residue involved in this step is Ser642 for the following reasons. First, the calculated position for the hydrogen on Cβ of isocitrate is directly juxtaposed to the OG atom of this serine (Figure 6a). Second, the OG atom of this serine resides in an environment surrounded by potential hydrogen bonds from the amide and guanidinium group of Arg644 (Figure 8). These interactions would stabilize a serine alkoxide and provide charge balance. Third, SO_4^{2-} binds in this region of the active site in the substrate-free enzyme (contacts from Arg644, Arg580, Gln72, and Ser643), showing affinity for two negative charges, i.e., the Cγ carboxyl of the substrate and the putative alkoxide. Together, these structural features argue that a Ser642 alkoxide is the base in the aconitase mechanism, in the sense that it accepts the conserved proton derived from Cβ of isocitrate. We wish to emphasize that aconitase employs a [4Fe–4S] cluster which can activate the bound substrate for proton and hydroxyl elimination or addition.

Water and Hydroxyl on Fe. Substrate-free aconitase has a hydroxyl ion bound to Fe4 (Fe_a) (Robbins & Stout, 1989b). Upon binding substrate, the hydroxyl is protonated to form H_2O (Werst et al., 1990a) as the Fe expands its coordination sphere (Telser et al., 1986). Following or simultaneous with proton abstraction from Cβ of isocitrate (Cα of citrate), the hydroxyl of substrate is eliminated to form *cis*-aconitate. Substrate oxygen derived from this hydroxyl is known to exchange with solvent H_2O (Telser et al., 1986; Rose & O'Connell, 1966). Therefore, both oxygen atoms (OHA and Ow) bound initially as hydroxyl groups must be protonated, and presumably also deprotonated, during turnover.

Figure 9 shows the hydrogen-bonding network surrounding these oxygen atoms. Hydrogens are included for modeling and refinement, but the distances indicated are for oxygen and nitrogen. Each oxygen (OHA and Ow) is in contact with a histidine (His101, His167), and the carboxylate of Asp165 contacts both oxygens simultaneously. His101 is paired with Asp100 and His167 with Glu262 (Figure 5) so that one could imagine each histidine being positively charged and capable of donating protons to OHA and Ow. Further, Asp165 is paired with His147 (Figure 5) so that this carboxylate could also participate in proton transfer steps important to the mechanism.

Substrate Recognition. Figure 6a displays the contacts of aconitase with isocitrate. Altogether, there are 18 potential hydrogen bonds in addition to two covalent bonds to Fe. All seven oxygen atoms have specific contacts, and each carboxyl is paired with at least one arginine. The Cα carboxyl is doubly hydrogen bonded to Arg452, as is the Cγ carboxyl to Arg580 (Figure 5). Arg644 has potential contacts to both of these carboxylates; in fact, the peptide SerSerArg644 involved in making an oxyanion hole (Figure 8) makes contacts to each carboxylate of isocitrate.

These contacts appear to be compatible with binding of citrate as well. On the basis of the spectroscopic and stereochemical data (Emptage, 1988) citrate is expected to bind via its Cβ carboxyl and hydroxyl such that Cα–H and Cβ–OH remain trans and only the acetyl arm is repositioned. A model for citrate built in this way has no bad contacts; in Figure 5a this would entail shifting the Cγ carboxyl, shown in contact to Arg580, to the adjacent carbon carrying the hydroxyl group. Contacts to Arg644 may be lost, but contacts to Arg580 and Gln72 could still be made. In other words, the enzyme may need only to "wobble" (as in GU vs GC base pairing) in order to recognize citrate vs isocitrate. Together these interactions should be more than enough to account for the stereospecific activity of aconitase on the prochiral substrate, citrate (Ogston, 1948).

The specific contacts to isocitrate are supported by a network of hydrogen bonds between side chains in the active site and surrounding protein atoms. The side chains of Asp100 and His101, Asp165 and His147, and Glu262 and His167 are paired as noted. The carboxylate of Asp165 also has contacts to Gln72 (NE2) and the amide of His167. Three possible salt links are observed between side chains of Glu262 and Arg447,

Asp568 and Arg644, and Asp568 and Arg452 (Figure 5a). Interactions involving main-chain atoms include the following amides: Ser166 (to substrate), His167 (to Asp165), Ser642 (to Thr567), Ser643 (to substrate), and Arg644 (to Ser642). The following carbonyls are involved in hydrogen bonds: Ala74 (with Arg580), Cys424 (with Arg452), and Ser571 (with Arg644). A string of Asn side-chain hydrogen bonds has been observed (Robbins & Stout, 1989a) for residues 170, 258, and 446; in the present structure, Thr 359 intervenes between Asn258 and Asn446. Aside from the OB2···Ow–Fe contact, substrate is excluded from solvent. However, the active site residues listed here have 12 contacts with ordered H_2O molecules in the cleft (Figure 1). A final type of interaction of potential importance is stacking of the side chains of Gln72 on His101, Asn446 on His167, and Asp165 on the Cβ carboxyl of isocitrate.

Discussion

The focus of this study is the elucidation of the catalytic mechanism of aconitase. The enzyme employs an Fe–S cluster and the role of the cluster in catalysis has been the subject of many investigations (Beinert & Kennedy, 1989). The reactions catalyzed are essential to basic energy metabolism. Our approach has been to prepare crystals of the wild-type enzyme grown in the presence of substrates and inhibitors. An independent study involves preparation of site-directed mutants suggested from the crystal structure using the cloned pig heart aconitase cDNA (Zheng et al., 1990) and assay of these mutants for activity (Zheng et al., 1992). Together, these studies are relevant to the mechanism of other dehydratases as well and may be important to understanding the activity of IRE-binding proteins, a growing class of recognized regulatory RNA-binding proteins (Rouault et al., 1991; Dandekar et al., 1991).

In this paper we have presented information on the crystal structures of aconitase in which isocitrate and nitroisocitrate are bound in the active site. The structures suggest two basic features of the mechanism: that Ser642 residing in an oxyanion hole is the base involved in abstraction of a proton from Cβ of substrate and that a network of interactions constructed of three histidines and three carboxylates is utilized for proton transfer steps involving two oxygen atoms bound to Fe, one derived from substrate hydroxyl and one from solvent.

Proton transfer steps are necessary for both substrate binding and catalysis. To illustrate these interactions, possible but speculative reaction schemes are presented. Figure 10 depicts the transition from the substrate-free, hydroxyl-bound, four-coordinate Fe state (Robbins & Stout, 1989b) to the substrate- and H_2O-bound, six-coordinate Fe state. Protonation of solvent-derived hydroxyl is observed in ENDOR experiments (Werst et al., 1990a) maintaining the same net charge on Fe after substrate binds. Figure 10 assumes that the proton derived from Ser642 to form an alkoxide is formally equivalent to the proton added to Fe–OH. To facilitate proton shifts the histidine–carboxylate pairs could donate/accept protons as observed in reactions catalyzed by serine proteases (Sprang et al., 1987), lipases (Schrag et al., 1991), and xylose isomerase (Whitlow et al., 1991). It is of interest to note that *Pyrococcus furiosus* ferredoxin, which has a hydroxyl bound to its [4Fe–4S] cluster, also has an aspartate residue proximal in the sequence (Conover et al., 1991).

The model implies conformational change in that OH^-/H_2O must swing from a tetrahedrally bound position to the octahedrally bound position observed. H_2O may be able to move more freely in the Fe coordination sphere than OH^-. Repositioning of bound OH^-/H_2O could be facilitated by the side

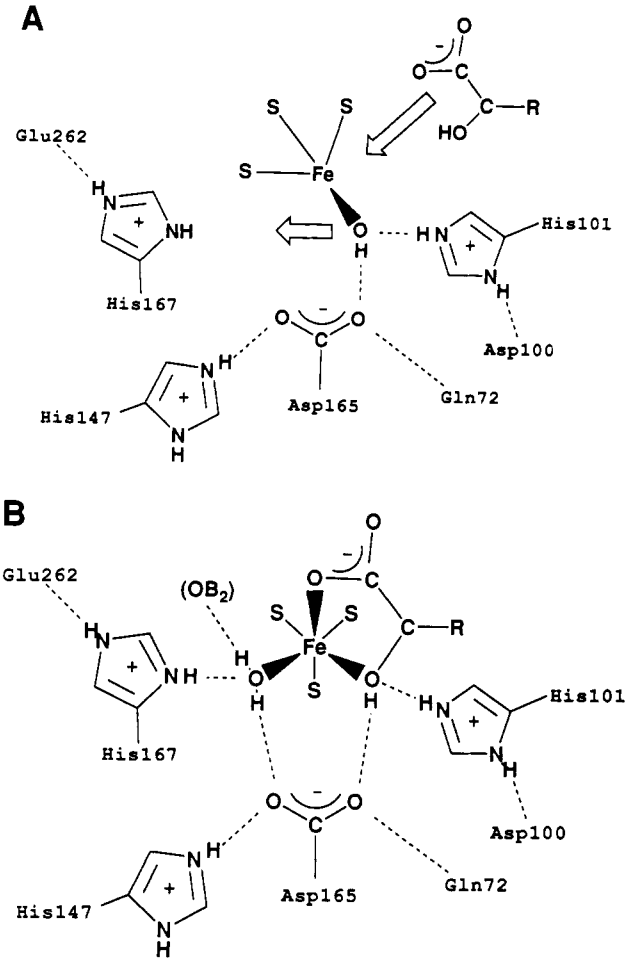

FIGURE 10: Schematic representation of the transition from substrate-free aconitase (A) to the substrate-bound form (B). The proton derived from Ser642 to form an alkoxide is formally equivalent to the proton added to Fe–Ow to make Fe–OH_2. The contact of Fe–OH_2 to Cβ carboxyl of substrate is shown separately for clarity. All three histidines are assumed to be protonated.

chain of Asp165, providing a hydrogen-bonded path between the two sites. Because the four- and six-coordinate Fe states of aconitase are observed in crystals of differing space group, our data cannot directly address the issue of conformational change in the protein upon substrate binding.

Figure 11 depicts a possible reaction sequence for isocitrate to *cis*-aconitate. The reaction is initiated by a Ser642 alkoxide. The serine is proposed to have a sufficiently lowered pK_a to be ionized when substrate binds and Fe-OH_2 is formed. The geometry of the contacts of Arg644 NE and amide to Ser642 OG is similar to the arrangement in chymotrypsin, where amides of Gly193 and Ser195 form an oxyanion hole (N···N distances 4.4 and 4.5 Å) (Fersht et al., 1973). In aconitase, Arg644 would provide additional charge stabilization for an alkoxide; there is also an Arg644 NH1 to OG contact. Arginines are utilized by carboxypeptidase (Phillips et al., 1990) and a catalytic antibody (Jackson et al., 1991) to stabilize reaction intermediates which are oxyanions. In a substrate-free form of aconitase crystals (Robbins & Stout, 1989a), sulfate binds to Arg644, Arg580, Ser643, and Gln72, suggesting an affinity for oxyanions in this region.

Transfer of the proton on Cβ to Ser642 creates the aci-acid intermediate mimicked by the ionized state of nitroisocitrate (Schloss et al., 1980) (Figure 11b). This intermediate collapses to *cis*-aconitate with cleavage of the Cα–OH bond (Figure 11c); protonation of substrate hydroxyl could occur by His101 as depicted (see also Figure 10b) or by Asp165. H_2O bound

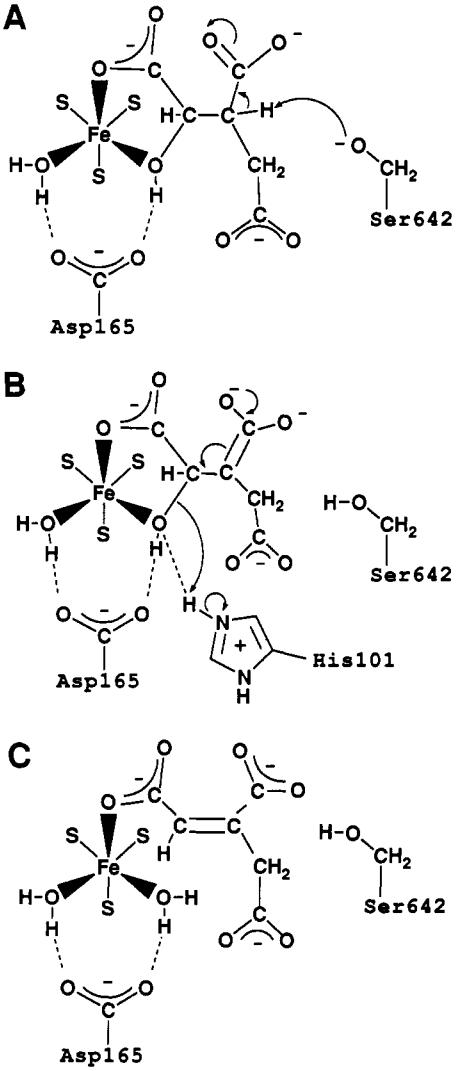

FIGURE 11: Schematic representation of the reaction isocitrate → *cis*-aconitate assuming deprotonation of Ser642 when substrate binds and Fe–OH_2 is formed. Formation of an aci-acid intermediate (A) and collapse of this intermediate (B) forms the product (C). Electron density could also flow from the Cβ–H bond to the Cα–Cβ double bond, i.e., directly from step A to C with concomitant cleavage of the Cα–OH bond.

to Fe can then exchange with solvent (Telser et al., 1986), while release of *cis*-aconitate may require deprotonation of bound H_2O to maintain a net charge in a reversal of the steps depicted in Figure 10. Displacement of *cis*-aconitate by another *cis*-aconitate molecule in the alternative binding mode flipped over 180° about the Cα–Cβ bond (Emptage, 1988), and reversal of the steps in Figure 11 forms citrate. In the presence of excess *cis*-aconitate, the Ser642 alkoxide, presumably with a relatively high pK_a, is the group that retains the substrate-derived proton (Rose & O'Connell, 1966).

Recently, it has been argued that removal of a proton from a carbon α to a carboxyl or carbonyl is too difficult for residues which are bases in enzymes, as the pK_as of these protons are very high. Consequently, abstraction actually may occur by concerted electrophilic catalysis (Gerlt et al., 1991). Such a possibility has been pointed out to explain the reactivity of the $[Co(en)_2(OH)(methylmaleato)]^+$ ion, a model compound for the aconitase reaction (Gahan et al., 1985). In aconitase, the Fe–S cluster can withdraw electron density (cleavage of Cα–OH bond), favoring the aci-acid intermediate (Figure 11b). The existence of this intermediate is supported by inhibition with the nitronate analogue (Schloss et al., 1980) which binds in a virtually identical manner to isocitrate. The aci-acid would be stabilized by contact to Arg447 and four hydrogen bonds from Ser166 and Ser643 (Figure 6a). Nevertheless, the structure also suggests a means of protonating the Cβ carboxyl as the OB2 atom is within hydrogen-bonding distance of Fe–OH_2 (Ow atom) (Figures 6a and 9). Transfer of a proton from Fe–OH_2 to the Cβ carboxyl (Fe–OH_2 + Cβ–COO^- → Fe–OH^- + Cβ–COOH), reprotonation of Fe–OH^- (see Figure 10), and a second proton transfer (Fe–OH_2 + Cβ–COOH → Fe–OH^- + Cβ–$COOH_2^+$) would create the enolate intermediate required for concerted electrophilic catalysis (Gerlt et al., 1991). The displaced Cβ proton would still have to reside on Ser642. Multiple proton transfers within the enzyme are implicated by the fact that three or more tritium atoms are trapped by aconitase exposed to high-activity [^{3}H]water prior to reaction with *cis*-aconitate (Kuo & Rose, 1987). However, proton transfers are also required in the formation of Fe–OH_2 (Figure 10).

The carbanion and electrophilic catalysis mechanisms can be viewed as equivalent if one detail of the structure is considered valid. In the structure of the enzyme with nitroisocitrate bound, the Fe_a–OH_2···Cβ carboxyl distance becomes 0.2 Å shorter compared to enzyme with isocitrate bound (Figure 6a,b; Ow–OB2 and Ow–ON2). The short 2.5-Å distance observed with the inhibitor suggests that this is a low-barrier hydrogen bond (Cleland, 1992), meaning that the proton is equally partitioned between both acceptor oxygens. In other words, the proton may both be transferred to the carboxyl group and resident on Fe–OH_2.

Why does aconitase contain an Fe–S cluster as opposed to a metal ion bound directly by protein side chains? One explanation would be that Fe coordinated by a [3Fe–4S] "ligand" is able to undergo the transformations from four- to six-coordination required, whereas other metals, such as Zn or Cu, or even Fe, bound by a minimum of three protein ligands, could not expand their coordination spheres to six. The H_2O ligand observed in aconitase with bound substrate is likely to be derived from the hydroxyl ligand in the substrate free enzyme; a Fe[3Fe–4S](OH) site (Figure 10a) is preferred over a tetrahedral Fe site at which a fourth protein ligand must be displaced. Consequently, H_2O is bound in addition to substrate, and the Fe coordination number becomes six. Further, the [3Fe–4S] "ligand" for Fe in aconitase provides steric freedom by removing the catalytic Fe 4.9 Å from the nearest protein ligands of the cluster (average Fe4···Sγ distance). The [4Fe–4S] cluster may also stabilize a carbanion intermediate more effectively than a single metal ion. Changes in the electronic environment of Fe in the cluster occur upon addition of substrate (Emptage et al., 1983; Kent et al., 1985).

The selection of the crystals (or the crystallization medium) for aconitase molecules with isocitrate bound prevents direct observation of citrate or *cis*-aconitate, at least in crystal forms available (Table I). These states will have to be approached using crystals grown from nitrocitrate (unpublished results), *trans*-aconitate, or a new crystal form. However, one substrate relevant to the present structure is α-methyl-*cis*-aconitate, which is converted only to α-methylisocitrate and not to α-methylcitrate (Schloss et al., 1984). A model of α-methylisocitrate constructed from isocitrate as observed in the active site (Figure 5a) has only three contacts of the methyl group carbon less than 3.5 Å to the enzyme: 3.2 Å to CG2 of Ile425, 3.3 Å to CD2 of His101, and 3.0 Å to NE2 of His101; the latter contact could be relieved by a small shift of this side chain. Thus the structure accommodates this methylated substrate. Without crystal structures of the enzyme in the

presence of other inhibitors (Table I), we cannot speculate about the inhibition by α-methylcitrate or other compounds.

Mitochondiral aconitase shares a striking homology with the RNA-binding protein, IRE-BP (Rouault et al., 1991). The conservation of all residues depicted in Figure 5, as well as those in sequences flanking active site residues, argues that IRE-BP is a cytosolic aconitase (Rouault et al., 1991). All insertions resulting from alignment of IRE-BP onto aconitase can be accommodated into the structure as expanded loops between conserved secondary structure elements. This is also true of the yeast aconitase sequence (Gangloff et al., 1990), where again all active site residues in the pig heart (isocitrate-bound) enzyme are conserved. It should be emphasized that the structure of the beef heart enzyme with nitroisocitrate bound presented here is based on homology with the pig heart sequence, as only 194 residues of the bovine enzyme have been determined by chemical means (see Experimental Procedures).

Isopropylmalate (IPM) isomerase catalyzes a reversible dehydration/rehydration step in leucine biosynthesis. The reaction is equivalent to the aconitase reaction except that the "acetyl arm" [$CH_2(\gamma)$–COOH] of isocitrate/citrate is replaced by an isopropyl group. The *Salmonella typhimurium* enzyme large subunit (Rosenthal & Calvo, 1990) is homologous to aconitase and shares 13 of 14 active site residues in the first three domains (Gln72 becomes His), including the AspSerHis167 sequence and the Cys ligands; the small subunit (Friedberg et al., 1985) apparently corresponds to the hinged fourth domain of aconitase and contains the SerSerArg644 sequence. The IPM isomerase from *Mucor circinelloides* (Roncero et al., 1989) is also homologous with aconitase; again 13 of 14 active site residues in the first three domains are the same. These homologies argue for the importance of the residues ascribed to the mechanism.

A final point of interest is the similarity in the manner in which isocitrate is bound by aconitase and isocitrate dehydrogenase (IcDH) (Hurley et al., 1991). In IcDH the Cα carboxyl and hydroxyl are coordinated to Mg^{2+} in the same way as to the Fe4 site, the Cα carboxyl is doubly hydrogen bonded to an arginine equivalent to Arg452 and one oxygen of the Cα carboxyl has a contact equivalent to Arg644 (Figure 6a). The Cα hydroxyl, which is oxidized by IcDH, also has contacts to two aspartates, but unlike Asp165 in aconitase these side chains are chelates to the metal. Thus, the CαOH(COO^-) moiety of isocitrate is recognized in a very similar manner by two enzymes with dissimilar folds catalyzing different reactions.

Acknowledgments

We are indebted to E. Münck and B. G. Fox for Mössbauer experiments, W. W. Cleland, J. A. Gerlt, and D. Hilvert for discussions, H. Parge for assistance with the program MERLOT, J. Rini for assistance with the program INTREF, D. S. Goodsell for searching binding modes of isocitrate with the program AUTODOCK, and M. H. Emptage for pointing out the homology of aconitase to IPM isomerases.

References

Beinert, H. (1990) *FASEB J. 4*, 2483–2491.

Beinert, H., & Thomson, A. J. (1983) *Arch. Biochem. Biophys. 222*, 333–361.

Beinert, H., & Kennedy, M. C. (1989) *Eur. J. Biochem. 186*, 5–15.

Beinert, H., Emptage, M. H., Dreyer, J.-L., Scott, R. A., Hahn, J. E., Hodgson, K. O., & Thomson, A. J. (1983) *Proc. Natl. Acad. Sci. U.S.A. 80*, 393–396.

Brünger, A. T., Karplus, M., & Petsko, G. A. (1989) *Acta Crystallogr. A45*, 50–61.

Carrell, H. L., Glusker, J. P., Villafranca, J. J., Mildvan, A. S., Dummel, R. J., & Kun, E. (1970) *Science 170*, 1412–1414.

Carter, C. W. (1977) in *Iron–Sulfur Proteins* (Lovenberg, W., Ed.) Vol. III, pp 158–204, Academic Press, New York.

Casey, J. L., Hentze, M. W., Koeller, D. M., Caughman, S. W., Rouault, T. A., Klausner, R. D., & Harford, J. B. (1988) *Science 240*, 924–928.

Cleland, W. W. (1992) *Biochemistry 31*, 317–319.

Conover, R. C., Park, J. B., Adams, M. W. W., & Johnson, M. K. (1991) *J. Am. Chem. Soc. 113*, 2799–2800.

Dandekar, T., Stripecke, R., Gray, N. K., Goossen, B., Constable, A., Johansson, H. E., & Hentze, M. W. (1991) *EMBO J. 10*, 1903–1909.

Emptage, M. H. (1988) in *Metals Cluster in Proteins* (Que, L., Ed.) pp 343–371, American Chemical Society, Washington, D.C.

Emptage, M. H., Kent, T. A., Kennedy, M. C., Beinert, H., & Münck, E. (1983) *Proc. Natl. Acad. Sci. U.S.A. 80*, 4674–4678.

Fersht, A. R., Blow, D. M., & Fastrez, J. (1973) *Biochemistry 12*, 2035.

Fitzgerald, P. M. D. (1988) *J. Appl. Crystallogr. 21*, 273–278.

Friedberg, D., Rosenthal, E. R., Jones, J. W., & Calvo, J. M. (1985) *Mol. Gen. Genet. 199*, 486–494.

Gahan, L. R., Harrowfield, J. M., Herlt, A. J., Lindoy, L. F., Whimp, P. O., & Sargeson, A. M. (1985) *J. Am. Chem. Soc. 107*, 6231–6242.

Gangloff, S. P., Marguet, D., & Lauquin, G. J.-M. (1990) *Mol. Cell. Biol. 10*, 3551–3561.

Gerlt, J. A., Kozarich, J. W., Kenyon, G. L., & Gassman, P. G. (1991) *J. Am. Chem. Soc. 113*, 9667–9669.

Glusker, J. G. (1971) in *The Enzymes* (Boyer, P. D., Ed) Vol. 5, pp 413–439, Academic Press, New York.

Goodsell, D. S., & Olson, A. J. (1990) *Proteins 8*, 195–202.

Haile, D. J., Hentze, M. W., Rouault, T. A., Harford, J. B., & Klausner R. D. (1989) *Mol. Cell. Biol. 9*, 5055–5061.

Houseman, A. L. P., Oh, B.-H., Kennedy, M. C., Fan, C., Werst, M. M., Beinert, H., Markley, J. L., & Hoffman, B. M. (1992) *Biochemistry* (in press).

Howard, A. J., Nielsen, C., & Xuong, N. H. (1985) in *Diffraction Methods for Biological Macromolecules* (Wyckoff, H. W., Hirs, C. H. W., & Timasheff, S. N., Eds.) pp 452–471, Academic Press, New York.

Hurley, J. H., Dean, A. M., Koshland, D. E., & Stroud, R. M. (1991) *Biochemistry 30*, 8671–8678.

Jackson, D. Y., Prudent, J. R., Baldwin, E. P., & Schultz, P. G. (1991) *Proc. Natl. Acad. Sci. U.S.A. 88*, 58–62.

Kaptain, S., Downey, W. E., Tang, C., Philpott, C., Haile, D., Orloff, D. G., Harford, J. B., Rouault, T. A., & Klausner, R. D. (1991) *Proc. Natl. Acad. Sci. U.S.A. 88*, 10109–10113.

Kennedy, M. C., Emptage, M. H., Dreyer, J. L., & Beinert, H. (1983) *J. Biol. Chem. 258*, 11098–11105.

Kennedy, M. C., Werst, M., Telser, J., Emptage, M. H., Beinert, H., & Hoffman, B. M. (1987) *Proc. Natl. Acad. Sci. U.S.A. 84*, 8854–8858.

Kent, T. A., Dreyer, J.-L., Kennedy, M. C., Huynh, B. H., Emptage, M. H., Beinert, H., & Münck, E. (1982) *Proc. Natl. Acad. Sci. U.S.A. 79*, 1096–1100.

Kent, T. A., Emptage, M. H., Merkle, H., Kennedy, M. C., Beinert, H., & Münck, E. (1985) *J. Biol. Chem. 260*, 6871–6881.

Klausner, R. D., & Harford, J. B. (1989) *Science 246*, 870-872.
Koeller, D. M., Casey, J. L., Hentze, M. W., Gerhardt, E. M., Chan, L. L., Klausner, R. D., & Harford, J. B. (1989) *Proc. Natl. Acad. Sci. U.S.A. 86*, 3574-3578.
Kuo, D. J., & Rose, I. A. (1987) *Biochemistry 26*, 7589-7596.
Luzzati, V. (1953) *Acta Crystallogr. 6*, 142.
Matthews, B. W. (1968) *J. Mol. Biol. 33*, 491-497.
Ogston, A. G. (1948) *Nature 162*, 963.
Plank, D. W., & Howard, J. B. (1988) *J. Biol. Chem. 263*, 8184-8189.
Phillips, M. A., Fletterick, R., & Rutter, W. J. (1990) *J. Biol. Chem. 265*, 20692-20698.
Robbins, A. H., & Stout, C. D. (1985) *J. Biol. Chem. 260*, 2328-2333.
Robbins, A. H., & Stout, C. D. (1989a) *Proteins 5*, 289-312.
Robbins, A. H., & Stout, C. D. (1989b) *Proc. Natl. Acad. Sci. U.S.A. 86*, 3639-3643.
Robbins, A. H., Stout, C. D., Piszkiewicz, D., Gawron, O., Yoo, C. S., Wang, B. C., & Sax, M. (1982) *J. Biol. Chem. 257*, 9061-9063.
Roncero, M. I. G., Jepsen, L. P., Streman, P., & Heeswijick, R. V. (1989) *Gene 84*, 335-343.
Rose, I. A., & O'Connell, E. L. (1966) *J. Biol. Chem. 242*, 1870-1879.
Rosenthal, E. R., & Calvo, J. M. (1990) *Nucleic Acids Res. 18*, 3072.
Rouault, T. A., Tang, C. K., Kaptain, S., Burgess, W. H., Haile, D. J., Samaniego, F., McBride, O. W., Harford, J. B., & Klausner, R. D. (1990) *Proc. Natl. Acad. Sci. U.S.A. 87*, 7958-7962.
Rouault, T. A., Stout, C. D., Kaptain, S., Harford, J. B., & Klausner, R. D. (1991) *Cell 64*, 881-883.
Schloss, J. V., Porter, D. J. T., Bright, H., & Cleland, W. W. (1980) *Biochemistry 19*, 2358-2362.
Schloss, J. V., Emptage, M. H., & Cleland, W. W. (1984) *Biochemistry 23*, 4572-4580.
Schrag, J. D., Li, Y., Wu, S., & Cygler, M. (1991) *Nature 351*, 761-764.
Sprang, S., Standing, T., Fletterick, R. J., Stroud, R. M., Finer-Moore, J., Xuong, N. H., Hamlin, R., Rutter, W. J., & Craik, C. S. (1987) *Science 237*, 905-909.
Switzer, R. L. (1989) *BioFactors 2*, 77-86.
Telser, J., Emptage, M. H., Merkle, H., Kennedy, M. C., Beinert, H., & Hoffman, B. M. (1986) *J. Biol. Chem. 261*, 4840-4846.
Walsh, C. (1979) in *Enzymatic Reaction Mechanisms*, pp 525-532, W. H. Freeman and Co., San Francisco, CA.
Werst, M. M., Kennedy, M. C., Beinert, H., & Hoffman, B. M. (1990a) *Biochemistry 29*, 10526-10532.
Werst, M. M., Kennedy, M. C., Houseman, A. L. P., Beinert, H., & Hoffman, B. M. (1990b) *Biochemistry 29*, 10533-10540.
Whitlow, M., Howard, A. J., Finzel, B. C., Poulos, T. L., Winborne, E., & Gilliland, G. L. (1991) *Proteins 9*, 153-173.
Yeates, T. O., & Rini, J. M. (1990) *Acta Crystallogr. A46*, 352-359.
Zheng, L., Andrews, P. C., Hermodson, M. A., Dixon, J. E., & Zalkin, H. (1990) *J. Biol. Chem. 265*, 2814-2821.
Zheng, L., Kennedy, M. C., Beinert, H., & Zalkin, H. (1992) *J. Biol. Chem.* (in press).

Probing Dynamic Changes in rRNA Conformation in the 30S Subunit of the *Escherichia coli* Ribosome†

Jennifer W. Weller and Walter E. Hill*
Division of Biological Sciences, University of Montana, Missoula, Montana 59812
Received July 9, 1991; Revised Manuscript Received January 6, 1992

ABSTRACT: Ribosomal RNA molecules within each ribosomal subunit are folded in a specific three-dimensional form. The accessibility of specific sequences of rRNA of the small ribosomal subunit of *Escherichia coli* was analyzed using complementary oligodeoxyribonucleotides, 6-15 nucleotides long. The degree of hybridization of these oligomers to their RNA complements within the 30S subunit was assessed using nitrocellulose membrane filter binding assays. Specifically, the binding of short DNA oligomers (hexameric and longer) complementary to nucleotides 919-928, 1384-1417, 1490-1505, and 1530-1542 of 16S rRNA was monitored, and in particular how such binding was affected by the change in the activation state of the subunit. We found that nucleotides 1397-1404 comprise an unusually accessible sequence in both active and inactive subunits. Nucleotides 919-924 are partially available for hybridization in active subunits and somewhat more so in inactive subunits. Nucleotides 1534-1542 are freely accessible in active, but only partially accessible in inactive subunits, while nucleotides 1490-1505 and 1530-1533 are inaccessible in both, under the conditions tested. These results are in general agreement with results obtained using other methods and suggest a significant conformational change upon subunit activation.

Within the 2 subunits of the *Escherichia coli* ribosome, there are over 50 different proteins and 3 rRNA molecules. It is becoming clear that the rRNA performs an active role in the ribosomal function. For instance, rRNA has been shown to have a role in mRNA placement (Shine & Dalgarno, 1974; Calogero et al., 1988) and tRNA alignment (Prince et al.,

† Supported by NIH Grant GM35717 to W.E.H.

0006-2960/92/0431-2748$03.00/0